

# Thermal behavior of the amorphous precursors of the $ZrO_2$ – $SnO_2$ system

Goran Štefanić\*, Svetozar Musić, Mile Ivanda

*Division of Materials Chemistry, Rugjer Bošković Institute, P.O. Box 180, HR-10002 Zagreb, Croatia*

Received 14 September 2007; received in revised form 21 November 2007; accepted 30 December 2007

Available online 5 January 2008

## Abstract

Thermal behavior of the amorphous precursors of the  $ZrO_2$ – $SnO_2$  system on the  $ZrO_2$ -rich side of the concentration range, prepared by co-precipitation from aqueous solutions of the corresponding salts, was monitored using differential thermal analysis, X-ray powder diffraction, Raman spectroscopy, field emission scanning electron microscopy (FE-SEM) and energy dispersive X-ray spectrometry (EDS). The crystallization temperature of the amorphous precursors increased with an increase in the  $SnO_2$  content, from 405 °C (0 mol%  $SnO_2$ ) to 500 °C (40 mol%  $SnO_2$ ). Maximum solubility of  $Sn^{4+}$  ions in the  $ZrO_2$  lattice (~25 mol%) occurred in the metastable products obtained upon crystallization of the amorphous precursors. A precise determination of unit-cell parameters, using both Rietveld and Le Bail refinements of the powder diffraction patterns, shows that the incorporation of  $Sn^{4+}$  ions causes an asymmetric distortion of the monoclinic  $ZrO_2$  lattice. The results of phase analysis indicate that the incorporation of  $Sn^{4+}$  ions has no influence on the stabilization of cubic  $ZrO_2$  and negligible influence on the stabilization of tetragonal  $ZrO_2$ . Partial stabilization of tetragonal  $ZrO_2$  in products having a tin content above its solid-solubility limit was attributed to the influence of  $ZrO_2$ – $SnO_2$  surface interactions. In addition to phases closely structurally related to cassiterite, monoclinic  $ZrO_2$  and tetragonal  $ZrO_2$ , a small amount of metastable  $ZrSnO_4$  phase appeared in the crystallization products of samples with 40 and 50 mol% of  $SnO_2$  calcined at 1000 °C. Further temperature treatments caused a decrease in and disappearance of metastable phases. The results of the micro-structural analysis show that the sinterability of the crystallization products significantly decreases with an increase in the  $SnO_2$  content.

© 2008 Elsevier Ltd. All rights reserved.

**Keywords:** A. Oxides; C. X-ray diffraction; C. Raman spectroscopy; C. Electron microscopy; D. Crystal structure; D. Microstructure

## 1. Introduction

High-temperature tetragonal (t-)  $ZrO_2$  (stable above 1170 °C) and cubic (c-)  $ZrO_2$  (stable above 2370 °C) could be stabilized at room temperature (RT) by incorporation of suitable aliovalent oversized cations ( $Y^{3+}$ ,  $Sc^{3+}$ ,  $Ca^{2+}$ , etc.), which decreased the  $Zr^{4+}$  coordination number by introduction of oxygen vacancies [1,2].

Incorporation of tetravalent cations does not introduce oxygen vacancies into the  $ZrO_2$  lattice. However, regardless of that, several studies have shown that the presence of tetravalent dopants, including oversized  $Ce^{4+}$  [3] and undersized  $Ge^{4+}$  and  $Ti^{4+}$  [4,5], could partially stabilize the tetragonal polymorph of zirconia. Li et al. have studied the effect of both oversized and undersized tetravalent dopants on the stabilization of high-temperature

\* Corresponding author. Tel.: +385 1 456 1111; fax: +385 1 468 0084.

E-mail address: [stefanic@rudjer.irb.hr](mailto:stefanic@rudjer.irb.hr) (G. Štefanić).

polymorphs of  $\text{ZrO}_2$  [6]. The authors concluded that undersized tetravalent dopants could only stabilize the tetragonal polymorph of zirconia, whereas oversized dopants, such as  $\text{Ce}^{4+}$ , could eventually stabilize even the cubic polymorph of  $\text{ZrO}_2$  when the cubic-like environment of the tetravalent dopants becomes the majority matrix [6].

There are several investigations related to the  $\text{ZrO}_2$ – $\text{SnO}_2$  system [7–14]. Hunter et al. [7–9] and Kim et al. [10] investigated the influence of  $\text{Sn}^{4+}$  ions incorporation into the tetragonal  $\text{ZrO}_2$ –2 mol%  $\text{Y}_2\text{O}_3$  system. The authors found that the replacement of  $\text{Zr}^{4+}$  ions with smaller  $\text{Sn}^{4+}$  ions caused an increase in the unit-cell volume of t- $\text{ZrO}_2$ -type solid solutions. Studies in the  $\text{ZrO}_2$ – $\text{SnO}_2$  phase diagram at high temperature (above 1000 °C) indicate that m- $\text{ZrO}_2 \rightarrow$  t- $\text{ZrO}_2$  transition upon heating and t- $\text{ZrO}_2 \rightarrow$  m- $\text{ZrO}_2$  transition upon cooling decreased with an increase in the tin content [10–12]. However, the presence of tin could not suppress the transition to a monoclinic polymorph of  $\text{ZrO}_2$  after cooling to room temperature. The investigation by Gaillard-Allemand et al. [11] has shown the existence of an immiscibility gap in the temperature range between 1230 and 1750 °C, leading to two  $\text{Zr}_{1-x}\text{Sn}_x\text{O}_2$  and  $\text{Sn}_{1-y}\text{Zr}_y\text{O}_2$  limited solid solutions. Kim et al. [10] estimated the solubility of  $\text{Sn}^{4+}$  ions in the  $\text{ZrO}_2$  lattice at  $\sim 8$  wt.% at 1500 °C. Wilson and Glasser [12] reported the appearance of a metastable  $\text{ZrSnO}_4$  phase, isomorphous with srilankite ( $\text{ZrTiO}_4$ ), in products having  $\sim 50$  mol% of  $\text{SnO}_2$  calcined at 1000 °C. This metastable phase decomposed during the prolonged calcination to a two-phase mixture consisting of a t- $\text{ZrO}_2$ -type solid solution containing  $\sim 10$  mol% of  $\text{SnO}_2$  and a cassiterite-type solid solution containing  $\sim 18$  mol% of  $\text{ZrO}_2$  [12]. Dhage et al. [13] reported a somewhat higher solubility of  $\text{Sn}^{4+}$  ions in the  $\text{ZrO}_2$  lattice. The solubility of  $\text{Sn}^{4+}$  ions in the m- $\text{ZrO}_2$  lattice was estimated at  $\sim 20$  mol% in the product obtained upon 15 h of calcination at 1000 °C. Recently, Ray et al. [14] reported that a cubic polymorph of  $\text{ZrO}_2$  was formed in the nanocrystalline powders of the  $\text{ZrO}_2$ – $\text{SnO}_2$  system obtained after crystallization of the amorphous precursors and cooling to room temperature. This report raises questions about the capability of undersized tetravalent cations to stabilize cubic polymorphs of  $\text{ZrO}_2$ .

In our previous investigations [15–18] we examined the effect of trivalent undersized dopant cations on the formation of high-temperature polymorphs of  $\text{ZrO}_2$ . The solubility of such dopants in products obtained upon calcination at high temperatures (above 1000 °C) is too small to stabilize high-temperature polymorphs of  $\text{ZrO}_2$ . However, it became significantly higher in metastable solid solutions obtained after crystallization of amorphous precursors (between 400 and 700 °C). The stabilization of high-temperature polymorphs of  $\text{ZrO}_2$  in such metastable systems occurs due to their extended capability for the formation of solid solutions. The obtained results show that  $\text{Fe}^{3+}$  ions could partially stabilize cubic polymorphs of  $\text{ZrO}_2$  when more than 20 mol% is incorporated [15]. The incorporation of smaller  $\text{Al}^{3+}$ ,  $\text{Cr}^{3+}$  or  $\text{Ga}^{3+}$  ions [16–18] partially stabilized only the tetragonal polymorph of  $\text{ZrO}_2$ . Partial stabilization of metastable t- $\text{ZrO}_2$  could also occur in products with negligible solubility of dopants due to strong surface interactions that prevent the diffusion of oxygen from the atmosphere into the  $\text{ZrO}_2$  lattice and trigger the t- $\text{ZrO}_2 \rightarrow$  m- $\text{ZrO}_2$  transition upon cooling [19].

In present investigation we examined thermal behavior of the amorphous precursors of the  $\text{ZrO}_2$ – $\text{SnO}_2$  system at the  $\text{ZrO}_2$ -rich side of the concentration region. The aim of the investigation was to find answers to questions about the maximum solubility of  $\text{Sn}^{4+}$  ions in a  $\text{ZrO}_2$  lattice, the influence of  $\text{Sn}^{4+}$  ions incorporation on the lattice parameters of  $\text{ZrO}_2$ -type solid solutions and the capability of  $\text{Sn}^{4+}$  ions to stabilize high-temperature tetragonal and cubic polymorphs of  $\text{ZrO}_2$ .

## 2. Experimental

Amorphous precursors of the  $\text{ZrO}_2$ – $\text{SnO}_2$  (ZS) system on the  $\text{ZrO}_2$ -rich side of the concentration range were co-precipitated from an aqueous solution of  $\text{ZrOCl}_2 \cdot 8\text{H}_2\text{O}$  (Aldrich) and  $\text{SnCl}_4 \cdot 5\text{H}_2\text{O}$  (Alfa Aesar) salts by adding 25%  $\text{NH}_3$  aq. up to pH = 10.3. All the chemicals were of analytical grade. The solid phase was separated from the corresponding liquid using an ultra-speed centrifuge, washed (five times with bidistilled water) then dried at 70 °C for 24 h. Dried samples were calcined at 400, 500, 700, 800, 1000 and 1200 °C for 2 h and analyzed at RT using X-ray powder diffraction, Raman spectroscopy, field emission scanning electron microscopy (FE-SEM) and energy dispersive X-ray spectrometry (EDS).

XRD measurements were taken using an ItalStructures diffractometer APD2000 with monochromatized Cu K $\alpha$  radiation (graphite monochromator). The positions of the diffraction lines of zincite (space group  $P6_3mc$ ,  $a = 3.24982(9)$  Å,  $c = 5.20661(15)$  Å) were used for the offset correction.

The crystallite size and micro-strain of the m-ZrO<sub>2</sub>-type solid solutions were estimated from the results of whole-powder-pattern profile refinements (Le Bail [20] method, program GSAS [21] with graphical user interface EXPGUI [22]) following the procedure proposed in the Size/Strain Round Robin [23].

Precise lattice parameters of m-ZrO<sub>2</sub>-type solid solutions were determined from the results of Le Bail [20] (program GSAS [21]) and Rietveld refinements [24] (program MAUD [25]) of powder diffraction patterns. Rietveld refinements of powder diffraction patterns were also used for a quantitative crystal phase analysis of the ZS products. In all the cases the  $R_{wp}$  indexes of the refined patterns were less than 10%. The obtained values of the volume fractions of t-ZrO<sub>2</sub>- and m-ZrO<sub>2</sub>-type solid solutions ( $\nu_t$  and  $\nu_m$ ) were compared with the values obtained from the integral intensities of monoclinic diffraction lines  $\bar{1}11$  and  $111$  and the tetragonal diffraction line  $101$ , following the procedure proposed by Toraya et al. [26]. Integrated intensities of the diffraction lines were determined using the individual profile-fitting method (program PRO-FIT [27]).

Raman scattering experiments were carried out at room temperature by using the double subtractive configuration of a Jobin Yvon T64000 triple monochromator. Within this configuration it is possible to obtain spectral information very close in to the laser line (to  $3\text{ cm}^{-1}$  in this experiment). The spectral resolution was  $1.4\text{ cm}^{-1}$ . The 514.5 nm laser excitation line beam of the coherent argon ion laser was focused on the diameter of  $5\text{ }\mu\text{m}$  by using  $100\times$  microscope objective. The laser power on the sample was 20 mW.

FE-SEM/EDS analyzes of uncoated samples were made using the field emission scanning electron microscope JSM-7000F (Jeol) equipped with an energy dispersive X-ray spectrometer INCA-350EDS Microanalysis System (Oxford Instruments).

Thermal behavior of the amorphous precursors of ZS systems was also examined by differential thermal analysis (DTA). Prepared samples were heated in an air atmosphere up to  $950\text{ }^\circ\text{C}$  at a rate of  $10\text{ }^\circ\text{C min}^{-1}$ , by using standard instrumentation.

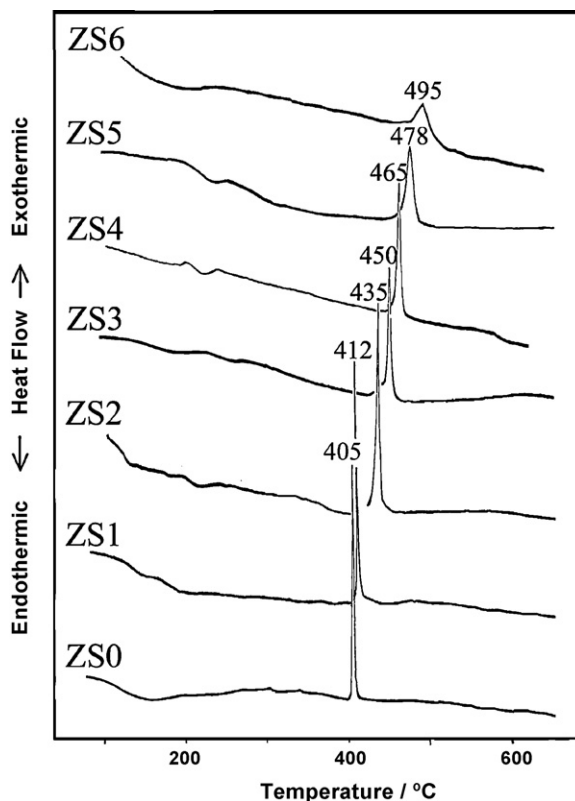


Fig. 1. DTA curves of samples from the ZrO<sub>2</sub>-SnO<sub>2</sub> system with a tin content between 0 and 40 mol% (Table 1).

### 3. Results and discussion

#### 3.1. Thermal behavior

DTA curves of samples from the  $\text{ZrO}_2\text{--SnO}_2$  system having a  $\text{SnO}_2$  content between 0 and 50 mol% are characterized by endothermic peaks resulting from dehydration, and exothermic peaks resulting from crystallization (Fig. 1). The position of the exothermic peak shifted to higher temperatures with an increase in the  $\text{SnO}_2$  content, from 405 °C for sample with 0 mol% of  $\text{SnO}_2$  to ~500 °C for sample with 40 mol% of  $\text{SnO}_2$  (Fig. 1). A comparison with the DTA results obtained for the systems  $\text{ZrO}_2\text{--M}_2\text{O}_3$  [15–18], where M stands for undersized trivalent cations ( $\text{Fe}^{3+}$ ,  $\text{Ga}^{3+}$ ,  $\text{Cr}^{3+}$  and  $\text{Al}^{3+}$ ), indicates that crystallization temperature of the amorphous co-gels depends on the amount of the dopant cation (crystallization temperature increases with an increase in the dopant content), ionic radius of the dopant cation (crystallization temperature increases with the increased difference in the ionic radii between the undersized dopant cation and  $\text{Zr}^{4+}$  ion) and the dopant cation valency (significantly smaller increase of the crystallization temperature for the  $\text{ZrO}_2\text{--SnO}_2$  system compared with the corresponding  $\text{ZrO}_2\text{--M}_2\text{O}_3$  systems) (Fig. 2).

#### 3.2. Phase analysis

Initial molar compositions and the results of phase analysis obtained upon calcination and cooling of the amorphous precursors of the  $\text{ZrO}_2\text{--SnO}_2$  (ZS) system are given in Table 1. X-ray diffraction patterns show that the phase structurally closely related to m- $\text{ZrO}_2$  is dominant in all crystallization products having an  $\text{SnO}_2$  content below 50 mol% (Fig. 3).

The first sign of the diffraction lines of the C phase, structurally closely related to an  $\text{SnO}_2$  phase cassiterite (space group  $P4_2/mmm$ ,  $a = 4.7382(4)$  Å,  $c = 3.1871(1)$  Å), appeared in the product of sample ZS5 (30 mol%  $\text{SnO}_2$ ) upon calcination at 500 °C (Fig. 4). Calcination temperature increased up to 800 °C caused an increase in the diffraction lines of the C phase, followed by the appearance and increase in the diffraction lines typical of high-temperature tetragonal or cubic polymorphs of  $\text{ZrO}_2$  (Fig. 4). These results indicate that the increased content of a metastable high-temperature  $\text{ZrO}_2$  polymorph is correlated with a decreased amount of  $\text{Sn}^{4+}$  ions incorporated into the  $\text{ZrO}_2$  lattice. Significant line broadening prevents clear distinguishing between the tetragonal and cubic polymorphs of  $\text{ZrO}_2$ .

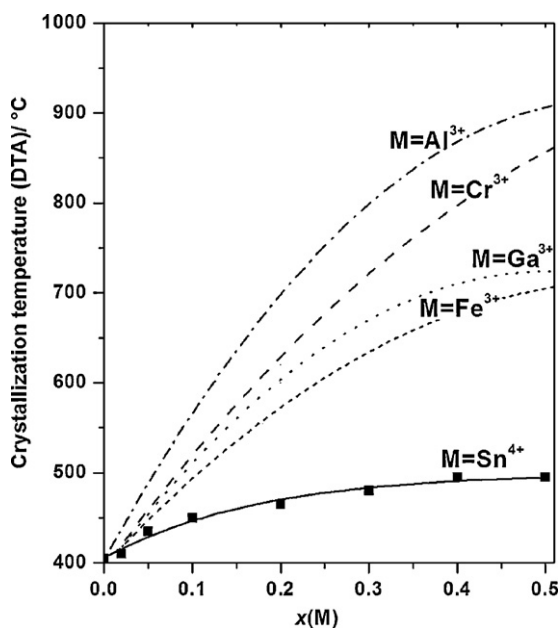


Fig. 2. The influence of the molar fraction of  $\text{Sn}^{4+}$  on the crystallization temperatures of the amorphous precursors of the  $\text{ZrO}_2\text{--SnO}_2$  system and the corresponding influences of trivalent undersized dopants ( $\text{Fe}^{3+}$ ,  $\text{Ga}^{3+}$ ,  $\text{Cr}^{3+}$  and  $\text{Al}^{3+}$ ).

Table 1

The initial molar compositions and the results of phase analysis obtained upon calcination (2 h) and cooling of the amorphous precursors of the  $\text{ZrO}_2\text{-SnO}_2$  system in the presence of air under atmospheric pressure

Sample	$x(\text{SnO}_2)$	$t$ ( $^\circ\text{C}$ )	Rietveld refinement, phase composition (volume fraction)	Individual profile fitting ( $v_m/v_m + v_r$ )
ZS0	–	400	m-ZrO <sub>2</sub> (0.55) + t-ZrO <sub>2</sub> (0.45)	0.67
		500	m-ZrO <sub>2</sub> (0.91) + t-ZrO <sub>2</sub> (0.09)	0.90
		700	m-ZrO <sub>2</sub> (0.98) + t-ZrO <sub>2</sub> (0.02)	0.99
		800	m-ZrO <sub>2</sub> (0.99) + t-ZrO <sub>2</sub> (0.01)	0.99
		1000	m-ZrO <sub>2</sub>	1
ZS1	0.02	500	m-ZrO <sub>2</sub> (0.89) + t-ZrO <sub>2</sub> (0.11)	0.91
		700	Z <sub>m</sub> (0.98) + Z <sub>t</sub> (0.02)	0.99
		800	Z <sub>m</sub>	1
		1000	Z <sub>m</sub>	1
		1200	Z <sub>m</sub>	1
ZS2	0.05	500	Z <sub>m</sub> (0.91) + Z <sub>t</sub> (0.09)	0.93
		700	Z <sub>m</sub> (0.98) + Z <sub>t</sub> (0.02)	0.99
		800	Z <sub>m</sub>	1
		1000	Z <sub>m</sub>	1
		1200	Z <sub>m</sub>	1
ZS3	0.10	500	Z <sub>m</sub> (0.87) + Z <sub>t</sub> (0.13)	0.87
		700	Z <sub>m</sub> (0.89) + Z <sub>t</sub> (0.01)	0.89
		800	Z <sub>m</sub> (0.91) + Z <sub>t</sub> (0.09)	0.93
		1000	Z <sub>m</sub> (0.95) + Z <sub>t</sub> (0.03) + C (0.02)	0.97
		1200	Z <sub>m</sub> + C (0.04)	1
ZS4	0.20	400	Z <sub>m</sub> (0.82) + Z <sub>t</sub> (0.18)	0.84
		500	Z <sub>m</sub> (0.81) + Z <sub>t</sub> (0.19)	0.84
		700	Z <sub>m</sub> (0.80) + Z <sub>t</sub> (0.20)	0.83
		800	Z <sub>m</sub> (0.79) + Z <sub>t</sub> (0.20) + C (0.01)	0.80
		1000	Z <sub>m</sub> (0.78) + Z <sub>t</sub> (0.11) + C (0.11)	0.90
ZS5	0.30	500	Z <sub>m</sub> (0.73) + Z <sub>t</sub> (0.22) + C (0.05)	0.84
		700	Z <sub>m</sub> (0.65) + Z <sub>t</sub> (0.28) + C (0.07)	0.77
		800	Z <sub>m</sub> (0.56) + Z <sub>t</sub> (0.32) + C (0.12)	0.57
		1000	Z <sub>m</sub> (0.60) + C (0.22) + Z <sub>t</sub> (0.18)	0.87
		1200	Z <sub>m</sub> + C	1
ZS6	0.40	500	Amorphous + Z <sub>m</sub> + Z <sub>t</sub> + C	0.62
		700	Z <sub>m</sub> (0.50) + Z <sub>t</sub> (0.33) + C (0.17)	0.62
		800	Z <sub>m</sub> (0.40) + Z <sub>t</sub> (0.37) + C (0.23)	0.52
		1000	Z <sub>m</sub> (0.44) + C (0.38) + Z <sub>t</sub> (0.14) + Z <sub>s</sub> (0.04)	0.87
		1200	Z <sub>m</sub> + C	1
ZS7	0.50	500	Amorphous + Z <sub>m</sub> + Z <sub>t</sub> + C	–
		700	Amorphous + Z <sub>t</sub> + Z <sub>m</sub> + C	–
		800	Amorphous + C + Z <sub>t</sub> + Z <sub>m</sub>	–
		1000	C (0.49) + Z <sub>m</sub> (0.29) + Z <sub>t</sub> (0.15) + Z <sub>s</sub> (0.07)	0.66
		1200	C + Z <sub>m</sub>	1

Description: Z<sub>m</sub> = phase structurally similar to m-ZrO<sub>2</sub>; Z<sub>s</sub> = phase structurally similar to orthorhombic ZrSnO<sub>4</sub>, Z<sub>t</sub> = phase structurally similar to t-ZrO<sub>2</sub>, C = phase structurally similar to t-SnO<sub>2</sub> (cassiterite).

In order to examine the capability of Sn<sup>4+</sup> ions to stabilize the cubic polymorph of ZrO<sub>2</sub>, Raman spectroscopy was used as the most powerful technique in cases where the tetragonal or cubic symmetry of ZrO<sub>2</sub> could not be clearly distinguished from the results of X-ray diffraction [28–30]. Group theory allows six Raman active modes of vibration ( $A_{1g} + 2B_{1g} + 3E_g$ ) for the tetragonal ZrO<sub>2</sub> polymorph, of which the band at  $\sim 265\text{ cm}^{-1}$  is usually used to determine the presence of a tetragonal phase, and only one active mode of vibration for the cubic polymorph ( $F_{2g}$ ) at  $\sim 610\text{ cm}^{-1}$ . Fig. 5 shows the Raman spectra of crystallization products from the ZrO<sub>2</sub>–SnO<sub>2</sub> system obtained upon calcination at 500 and 700  $^\circ\text{C}$ . Bands typical of m-ZrO<sub>2</sub> are present in all spectra. The increased amount of tin causes the appearance

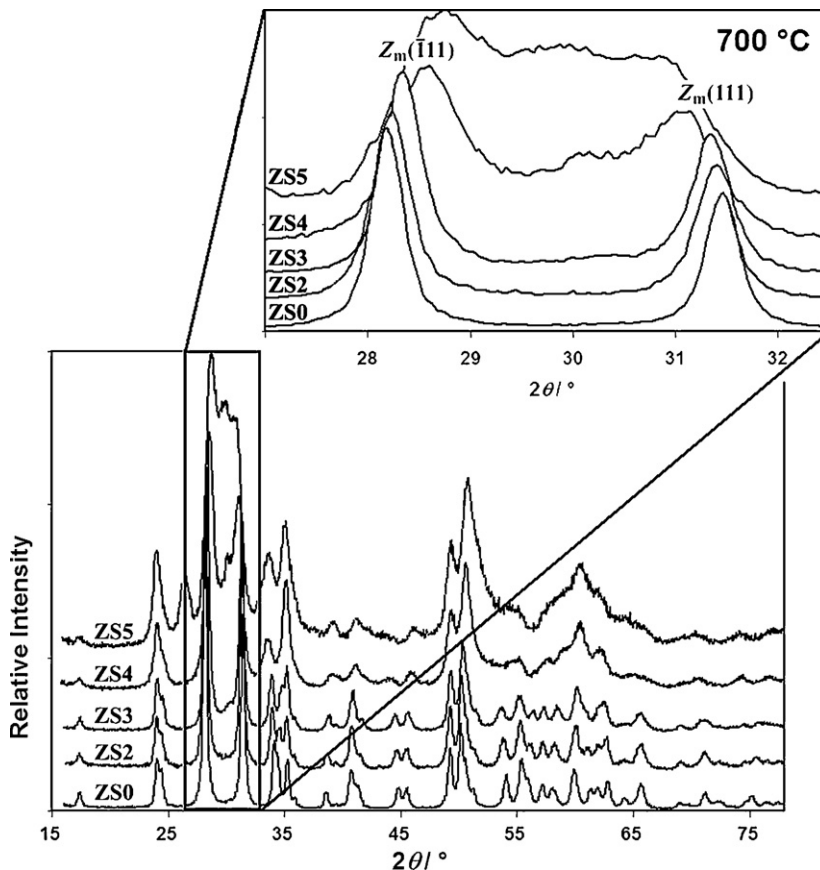


Fig. 3. XRD patterns of products from the  $\text{ZrO}_2\text{-SnO}_2$  system with a  $\text{SnO}_2$  content between 0 and 30 mol% (Table 1), obtained upon calcination at  $700\text{ }^\circ\text{C}$ .

of the band at  $\sim 265\text{ cm}^{-1}$ , which indicates that the observed high-temperature  $\text{ZrO}_2$  polymorph has a tetragonal symmetry.

Rietveld refinements (Fig. 6) of powder diffraction patterns were used to estimate volume fractions of the obtained crystalline phases (Table 1) and the solid-solubility limit of  $\text{Sn}^{4+}$  ions in a  $\text{ZrO}_2$  lattice. The results show the maximum

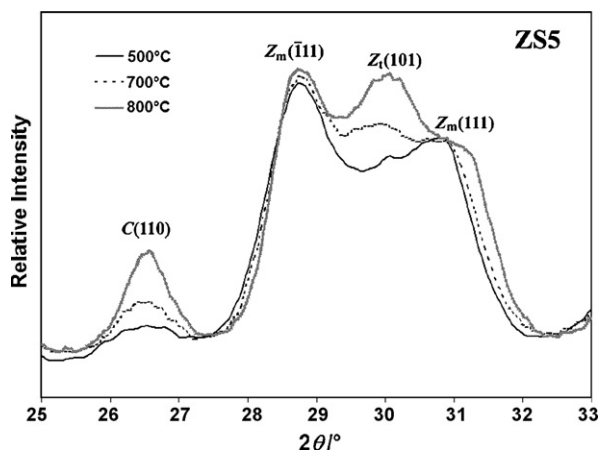


Fig. 4. Characteristic part of XRD patterns of products from the  $\text{ZrO}_2\text{-SnO}_2$  system with 30 mol% of  $\text{SnO}_2$  calcined at  $500\text{ }^\circ\text{C}$ ,  $700\text{ }^\circ\text{C}$  and  $800\text{ }^\circ\text{C}$ .

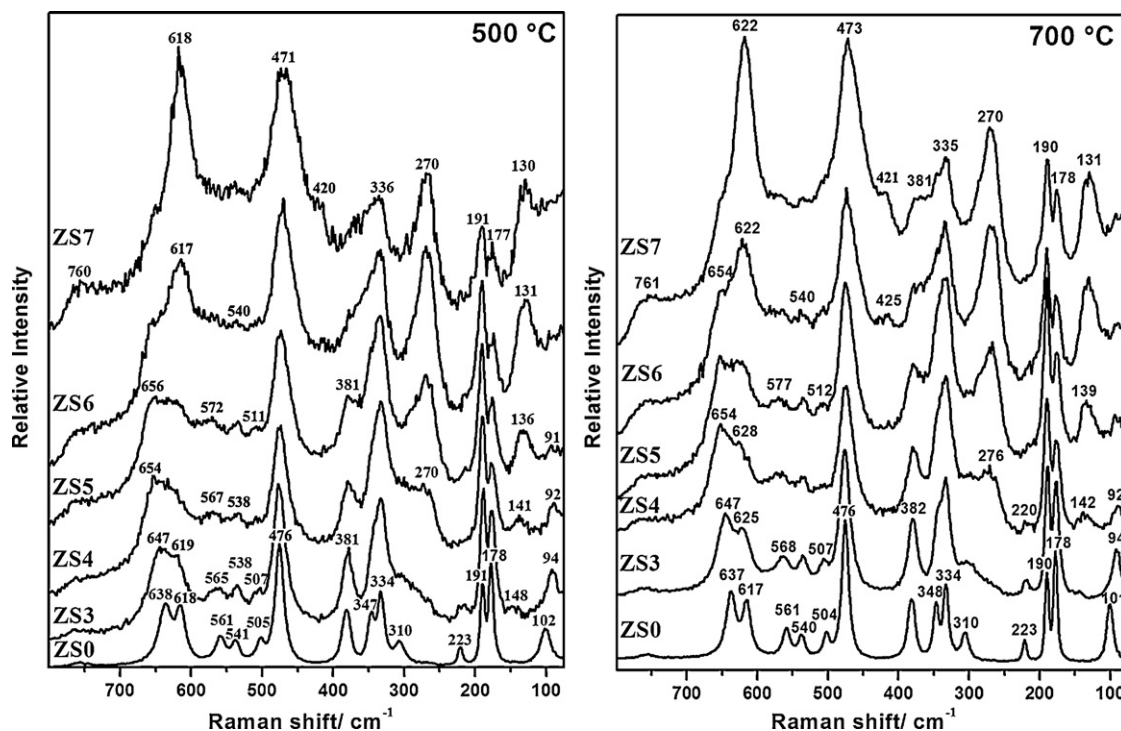


Fig. 5. Raman spectra of crystallization products from the  $\text{ZrO}_2\text{-SnO}_2$  system with a  $\text{SnO}_2$  content between 0 and 50 mol% (Table 1), obtained upon calcination at 500 °C and 700 °C.

solubility of  $\text{Sn}^{4+}$  ions in the  $m\text{-ZrO}_2$  lattice, estimated at  $\sim 25$  mol%, in a metastable solid solution obtained upon crystallization of the amorphous precursors. A rise in calcination temperature up to 800 °C leads to a decreased solid-solubility of  $\text{Sn}^{4+}$  ions followed by an increased amount of  $Z_t$  phase, structurally closely related to  $t\text{-ZrO}_2$ . The obtained ratios between the volume fractions of the  $Z_t$  and  $Z_m$  phases appeared to be in good agreement with the corresponding ratios obtained from the integral intensities of the monoclinic diffraction lines  $\bar{1}11$  and  $111$  and the tetragonal diffraction line  $101$ , following a procedure proposed by Toraya et al. [26].

Fig. 7 shows how the ratio between the volume fraction of  $Z_t$  phase and the sum of the volume fractions of  $Z_t$  and  $Z_m$  phases,  $v_t/(v_m + v_t)$ , varies with the amount of tin and calcination temperature (up to 800 °C). The products having a low amount of  $\text{SnO}_2$  (up to  $\sim 18$  mol%) exhibit regular behavior, calcination at lower temperature (500 °C) yields products having a higher amount of metastable tetragonal zirconia. In case of products having a higher amount of  $\text{SnO}_2$  (from 20 to 50 mol%) calcination at higher temperatures (700 and 800 °C) yields products having a higher amount of metastable tetragonal zirconia. The increase occurs approximately when the  $\text{SnO}_2$  content exceeds the solid-solubility limit, estimated at  $\sim 25$  mol% at 500 °C,  $\sim 22$  mol% at 700 °C, and  $\sim 18$  mol% at 800 °C (Fig. 7). These results indicate that the increased amount of  $Z_t$  phase in crystallization products calcined at 700 °C and 800 °C could not be attributed to the incorporation of  $\text{Sn}^{4+}$  ions into the  $\text{ZrO}_2$  lattice. Stabilization of the  $t\text{-ZrO}_2$  polymorph in these crystallization products probably results from a  $\text{ZrO}_2\text{-SnO}_2$  surface interaction, similarly as in the  $\text{ZrO}_2/\text{SO}_4^{2-}$  system [31], that prevents the diffusion of oxygen from the atmosphere into the  $\text{ZrO}_2$  lattice and triggers the  $t\text{-ZrO}_2 \rightarrow m\text{-ZrO}_2$  transition upon cooling. The surface interaction appeared to be a very important factor in stabilization of the  $t\text{-ZrO}_2$ -type phase in the crystallization products of  $\text{ZrO}_2\text{-MO}_x$  systems, such as  $\text{ZrO}_2\text{-CrO}_{1.5}$  [19],  $\text{ZrO}_2\text{-AlO}_{1.5}$  [16],  $\text{ZrO}_2\text{-NiO}$  [32] or  $\text{ZrO}_2\text{-SnO}_2$ . Due to surface interactions the amount of the  $t\text{-ZrO}_2$ -type phase in crystallization products of these systems increased with the increase in the  $\text{MO}_x$  content above the solubility limit of the corresponding metal cations in the  $\text{ZrO}_2$  lattice.

Calcination of the crystallization products of the  $\text{ZrO}_2\text{-SnO}_2$  system at 1000 °C caused an increase in the amount of  $Z_m$  and C phases and a decrease in the amount of metastable  $Z_t$  phase (Fig. 8). Diffraction patterns of samples ZS6 and ZS7 (40 and 50 mol% of  $\text{SnO}_2$ ), calcined at 1000 °C, contain additional diffraction lines that indicate the presence of a

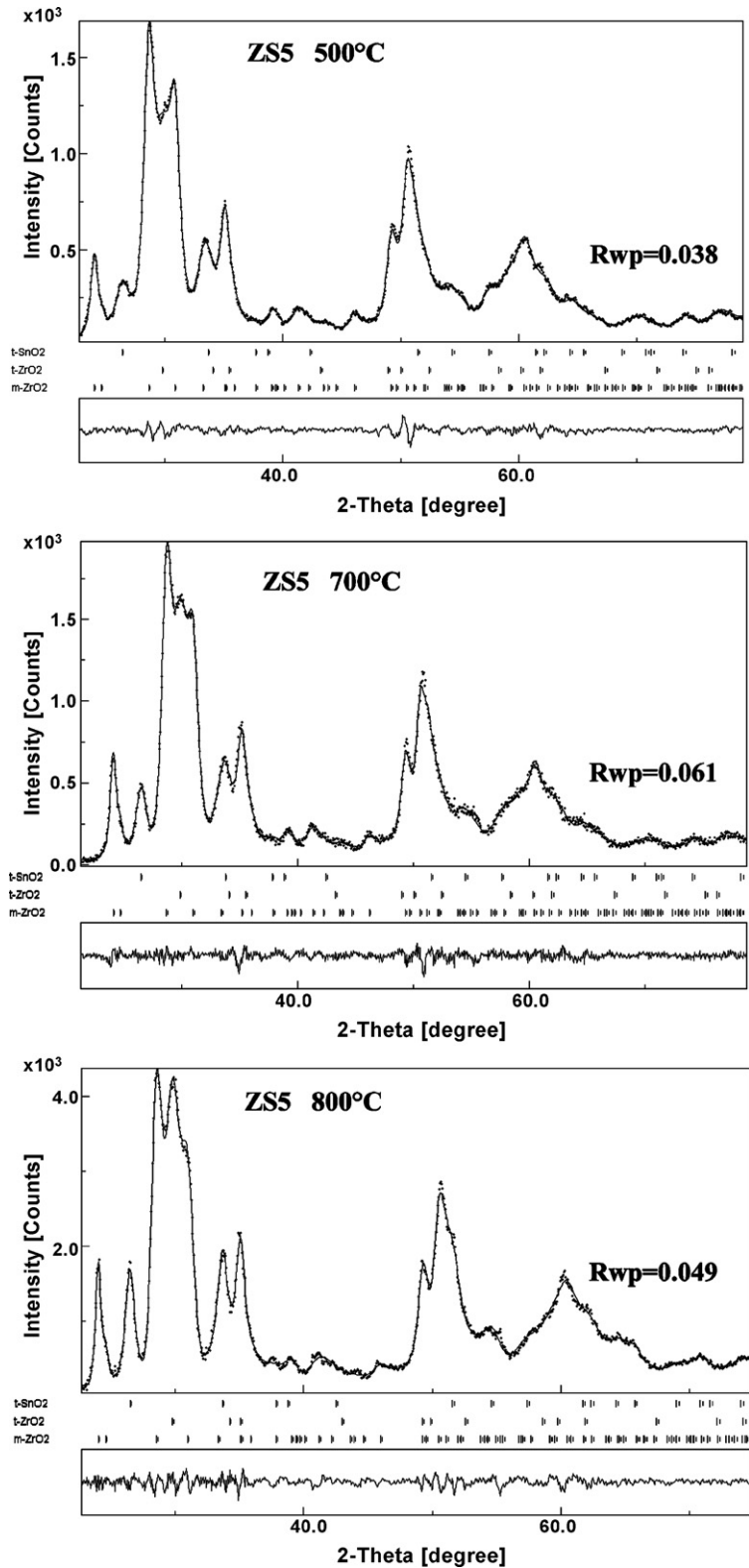


Fig. 6. The results of Rietveld refinements (MAUD program) of crystallization products from the  $ZrO_2$ - $SnO_2$  system with 30 mol% of  $SnO_2$  calcined at 500 °C, 700 °C and 800 °C. The differences between the observed and refined patterns are shown in the box below.

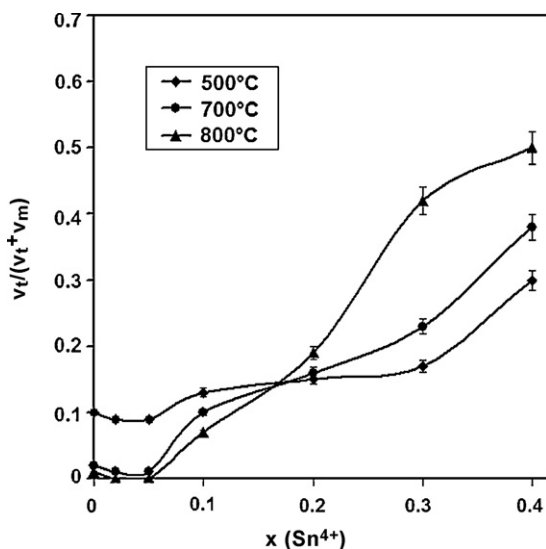


Fig. 7. The influence of the SnO<sub>2</sub> content on the ratio between the volume fraction of Z<sub>t</sub> phase and the sum of the volume fractions of Z<sub>t</sub> and Z<sub>m</sub> phase,  $v_t/(v_m + v_t)$ , in products calcined at 500 °C, 700 °C and 800 °C.

small amount of ZrSnO<sub>4</sub> phase (Fig. 8), first reported by Wilson and Glasser [12]. A possibility of the presence of a small amount of ZrSnO<sub>4</sub> phase in the crystallization product of sample ZS7 calcined at lower temperatures (700 and 800 °C) could not be completely excluded in view of the line broadening and a significant overlap between the diffraction lines of ZrSnO<sub>4</sub> phase and those of the other present phases (Z<sub>t</sub>, Z<sub>m</sub> and C phases). However, if present, the amount of this phase must be very small. Wilson and Glasser [12] indicated that a metastable ZrSnO<sub>4</sub> phase appears only in products calcined at 1000 °C or higher temperatures. The volume fraction of ZrSnO<sub>4</sub> phase in ZS6 and ZS7

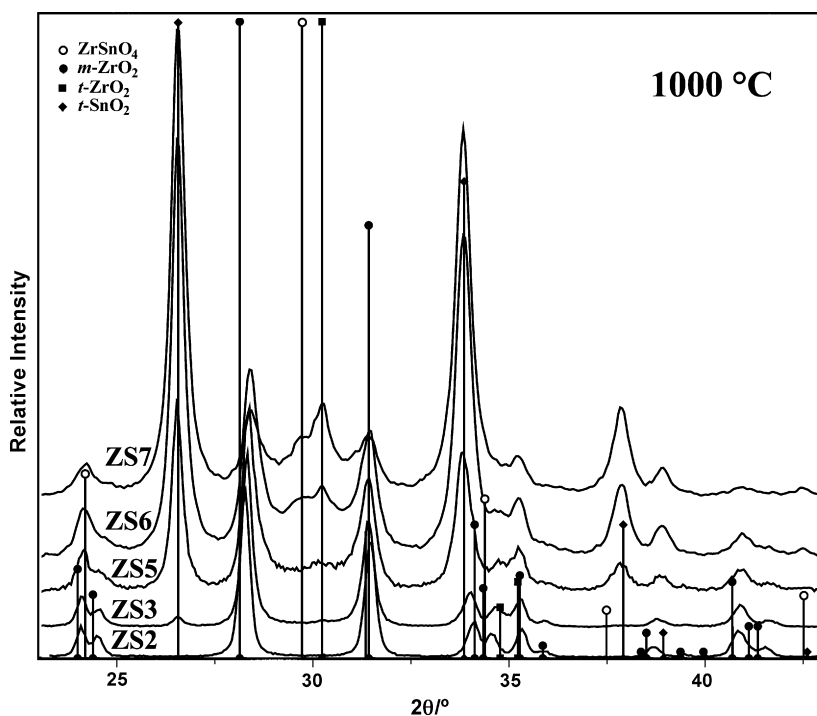


Fig. 8. Characteristic part of the diffraction patterns of ZS crystallization products obtained upon calcination at 1000 °C. Vertical lines mark the positions of the phases identified in these diffraction patterns.

products calcined at 1000 °C was estimated from the results of Rietveld refinements, performed on the assumption that a metastable  $\text{ZrSnO}_4$  phase is isomorphic with srilankite ( $\text{ZrTiO}_4$ ), to ~5%. Calcination at 1200 °C caused the disappearance of metastable  $\text{ZrSnO}_4$  and  $\text{Z}_1$  phases (Table 1).

### 3.3. Lattice parameters of $m\text{-ZrO}_2$ -type solid solutions

A closer look at the portion of the diffraction patterns of crystallization products calcined at 700 °C, containing the most prominent diffraction lines of  $m\text{-ZrO}_2$ , shows that an increase in the  $\text{SnO}_2$  content shifts the diffraction lines  $\bar{1}11$  and  $020$  to a higher angle, and the diffraction lines  $111$  and  $200$  to a lower angle, whereas the position of the diffraction line  $002$  remains almost unchanged (Fig. 9). These results indicate that the incorporation of  $\text{Sn}^{4+}$  ions causes an asymmetric distortion of the  $m\text{-ZrO}_2$  lattice.

Unit-cell parameters of the  $m\text{-ZrO}_2$ -type solid solutions were determined with precision from the results of Rietveld refinements [24] (MAUD program [25]) and Le Bail refinements [20] (GSAS program [21]) of powder diffraction patterns. Fig. 10 shows the observed and calculated powder patterns of crystallization products containing  $m\text{-ZrO}_2$ -type solid solutions with a varying tin content. The refined unit-cell parameters of the ZS product are listed in Table 2. The obtained results (Fig. 11) show that the increased amount of incorporated tin cations caused an increase in parameter  $a$ , a decrease in parameter  $b$ , a very small decrease in parameter  $c$  and a significant decrease in angle  $\beta$ . Similar results were obtained by Gaillard-Allemand et al. [11]. However, in this investigation the authors examined, *in situ*, a phase diagram of the  $\text{ZrO}_2\text{-SnO}_2$  system at very high temperatures (between 1230 and 1750 °C) with a significantly lower solubility of  $\text{Sn}^{4+}$  ions [11].

### 3.4. Micro-structural analysis

FE SEM micrographs show that, regardless of the amount of  $\text{SnO}_2$ , products obtained upon crystallization of amorphous precursors contain very small particles (~10 nm in size) of spherical morphology (Figs. 12 and 13). Temperature treatment leads to the crystallite growth and the reduction of porosity. However, an increase in the tin content caused a significant decrease in the sintering rate. The results of EDS analysis of all obtained products indicate presence of only three elements: Zr, Sn and O (no sign of Cl impurities). Zr/Sn ratios in samples, determined from the results of EDS analysis, appeared to be in good agreement with the Zr/Sn ratios in starting aqueous solutions. Upon calcination at 700 °C all samples appeared to be highly porous, with particle sizes between 20 and 30 nm. Upon

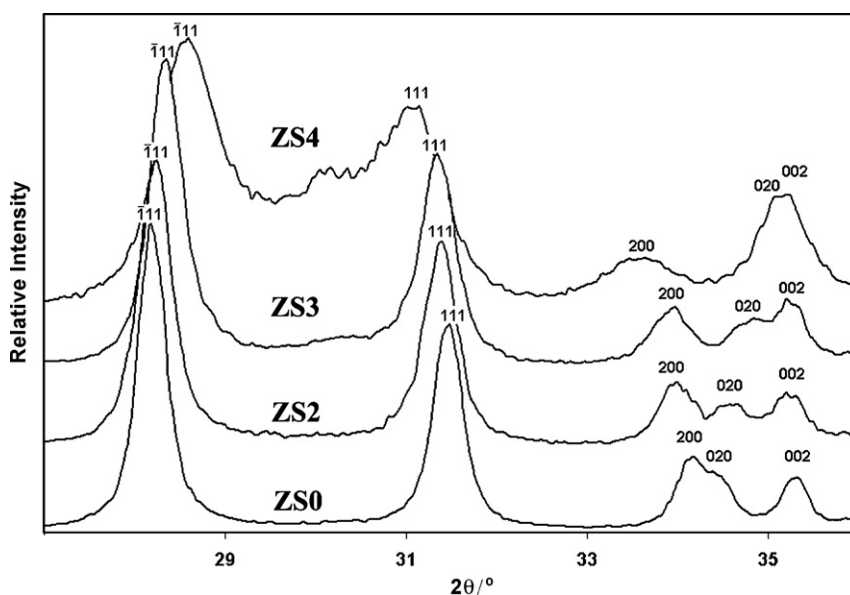


Fig. 9. Characteristic parts of the diffraction patterns of ZS crystallization products calcined at 700 °C having a  $\text{SnO}_2$  content between 0 and 20 mol% (Table 1), which contain the most prominent diffraction lines of  $m\text{-ZrO}_2$ .

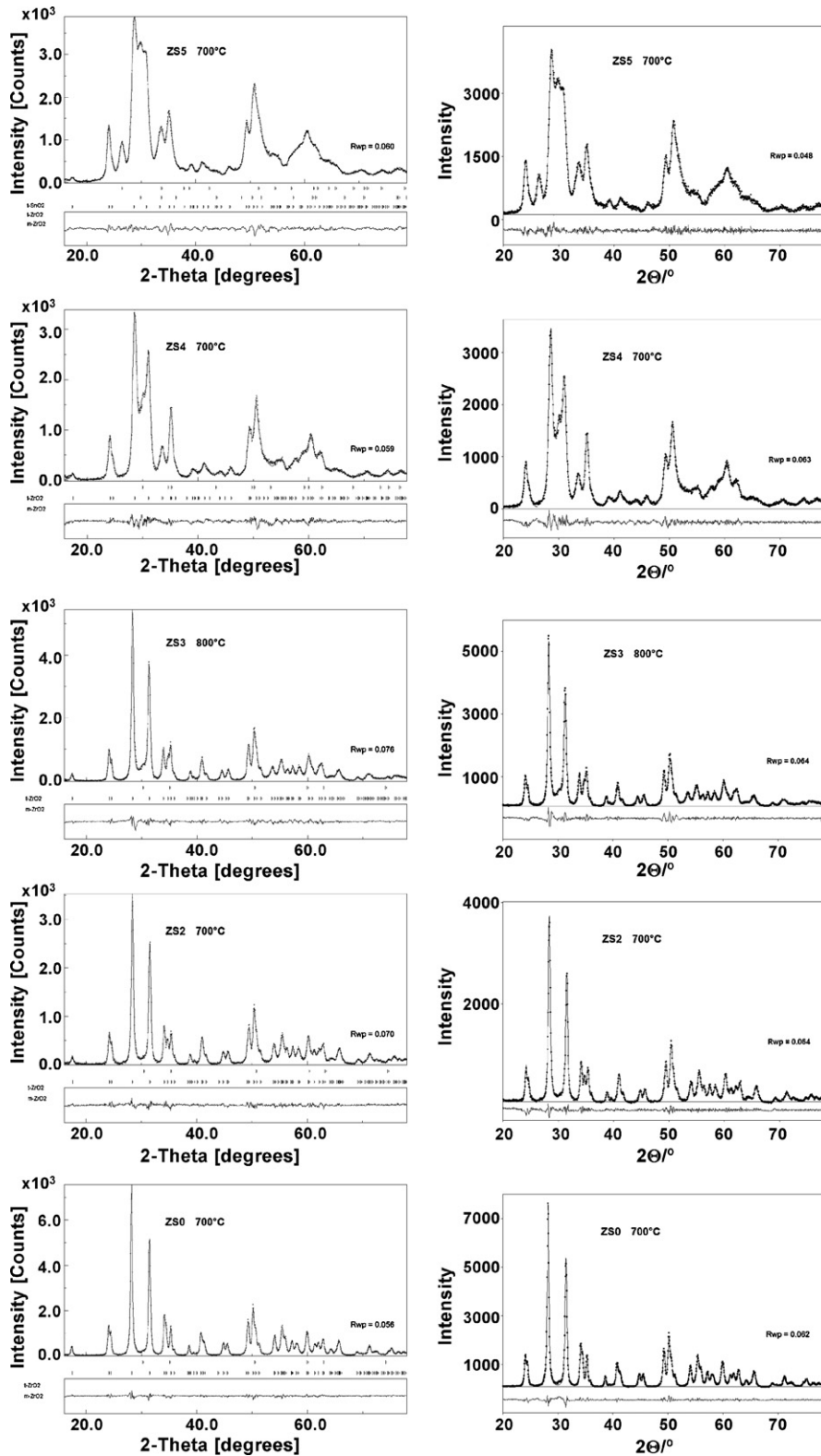


Fig. 10. The results of Rietveld (left) and Le Bail refinements (right) of crystallization products containing m-ZrO<sub>2</sub>-type solid solutions with different amounts of incorporated Sn<sup>4+</sup> ions. The difference between the observed and calculated patterns is shown as a line in the lower field.

Table 2

Refined values of the unit-cell parameters of m-ZrO<sub>2</sub>-type solid solutions, obtained upon crystallization of the amorphous precursors of ZrO<sub>2</sub>-SnO<sub>2</sub> systems, with varying amounts of incorporated Sn<sup>4+</sup> ions

Phase	<i>a</i> (Å)	<i>b</i> (Å)	<i>c</i> (Å)	$\beta$ (°)	<i>V</i> (Å <sup>3</sup> )	<i>R</i> <sub>wp</sub>
Le Bail refinement (GSAS program)						
m-ZrO <sub>2</sub>	5.3217(3)	5.1990(3)	5.1512(3)	99.195(4)	140.67	0.062
m-Zr <sub>0.98</sub> Sn <sub>0.02</sub> O <sub>2</sub>	5.3229(7)	5.1970(6)	5.1501(5)	99.077(6)	140.67	0.069
m-Zr <sub>0.95</sub> Sn <sub>0.05</sub> O <sub>2</sub>	5.3345(4)	5.1832(4)	5.1520(4)	98.890(6)	140.74	0.064
m-Zr <sub>0.90</sub> Sn <sub>0.10</sub> O <sub>2</sub>	5.3502(7)	5.1670(6)	5.1529(6)	98.556(6)	140.86	0.064
m-Zr <sub>0.80</sub> Sn <sub>0.20</sub> O <sub>2</sub>	5.3880(9)	5.1213(9)	5.1482(8)	97.270(9)	140.92	0.063
m-Zr <sub>0.77</sub> Sn <sub>0.23</sub> O <sub>2</sub>	5.4025(9)	5.0997(9)	5.1456(9)	96.740(9)	140.79	0.047
Rietveld refinement (MAUD program)						
m-ZrO <sub>2</sub>	5.3211(3)	5.2048(3)	5.1514(3)	99.173(3)	140.62	0.056
m-Zr <sub>0.98</sub> Sn <sub>0.02</sub> O <sub>2</sub>	5.3254(4)	5.1962(4)	5.1515(3)	99.062(5)	140.77	0.065
m-Zr <sub>0.95</sub> Sn <sub>0.05</sub> O <sub>2</sub>	5.3352(6)	5.1831(6)	5.1504(6)	98.891(6)	140.71	0.070
m-Zr <sub>0.90</sub> Sn <sub>0.10</sub> O <sub>2</sub>	5.3489(5)	5.1667(5)	5.1503(4)	98.495(7)	140.77	0.076
m-Zr <sub>0.80</sub> Sn <sub>0.20</sub> O <sub>2</sub>	5.3892(12)	5.1204(13)	5.1456(13)	97.214(16)	140.87	0.059
m-Zr <sub>0.77</sub> Sn <sub>0.23</sub> O <sub>2</sub>	5.4026(20)	5.1065(18)	5.1396(14)	96.583(36)	140.92	0.060
m-Zr <sub>0.75</sub> Sn <sub>0.25</sub> O <sub>2</sub>	5.4127(19)	5.0930(15)	5.1405(14)	96.446(22)	140.81	0.037

calcination at 1000 °C the sintering process caused a close interconnection of the crystallites (~100 nm in size) of pure ZrO<sub>2</sub>. Further calcination (1200 °C) caused the growth of these crystallites to several hundred nanometers (Fig. 12). Unlike pure ZrO<sub>2</sub>, crystallization products of samples that contain tin are still highly porous upon calcination at 1000 °C. A close interconnection of crystallites (~200 nm in size) of sample ZS3 (10 mol% of SnO<sub>2</sub>) occurs upon calcination at 1200 °C. However, a few pores are still present (Fig. 12). A decrease of sinterability becomes much more pronounced in the crystallization products of samples with a higher tin content. Even after calcination at 1200 °C the crystallization products of samples ZS5 (30 mol% of SnO<sub>2</sub>) and ZS7 (50 mol% of SnO<sub>2</sub>) are highly porous (Fig. 13).

The results of Raman spectroscopy and X-ray powder diffraction were also used for micro-structural analysis of ZS crystallization products. Fig. 14 shows low frequency Raman (LFR) spectra, given in log–log coordinates, of the ZS products calcined at 500 and 700 °C. Raman spectra contain a humps at ~13 cm<sup>-1</sup> (500 °C) and at ~5 cm<sup>-1</sup> (700 °C) resulting from the acoustic vibrational modes of nanoparticles. The procedure for the evaluation of the particle size distribution from the shape of the LFR peaks is described in our previous paper [33] and here we will present only the

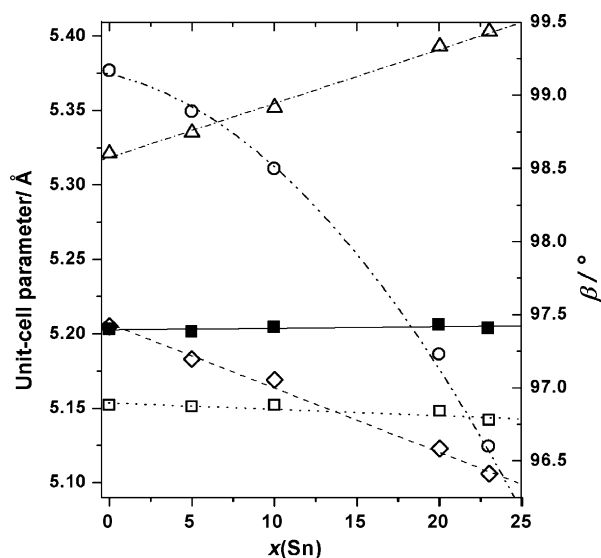


Fig. 11. Influence of the Sn<sup>4+</sup> ion content on parameter *a* (△), parameter *b* (◇), parameter *c* (□), angle  $\beta$  (○), and the cube root of the unit-cell volume (■) of the m-Zr<sub>1-x</sub>Sn<sub>x</sub>O<sub>2</sub> solid solution.

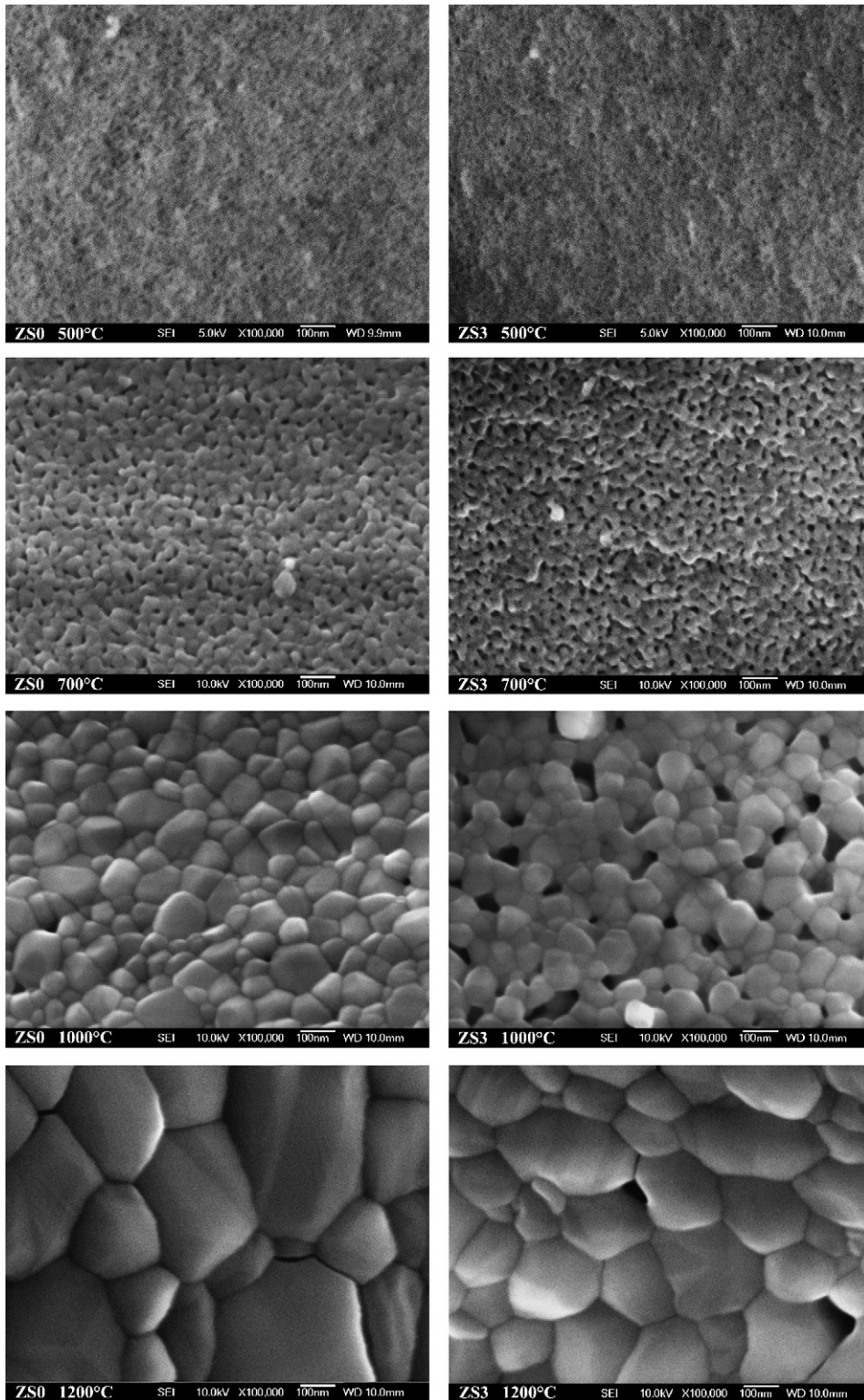


Fig. 12. FE-SEM micrographs of crystallization products from the  $\text{ZrO}_2\text{-SnO}_2$  system with 0 mol% (ZS0) and 10 mol% (ZS3) of  $\text{SnO}_2$  calcined at 500 °C, 700 °C, 1000 °C and 1200 °C.

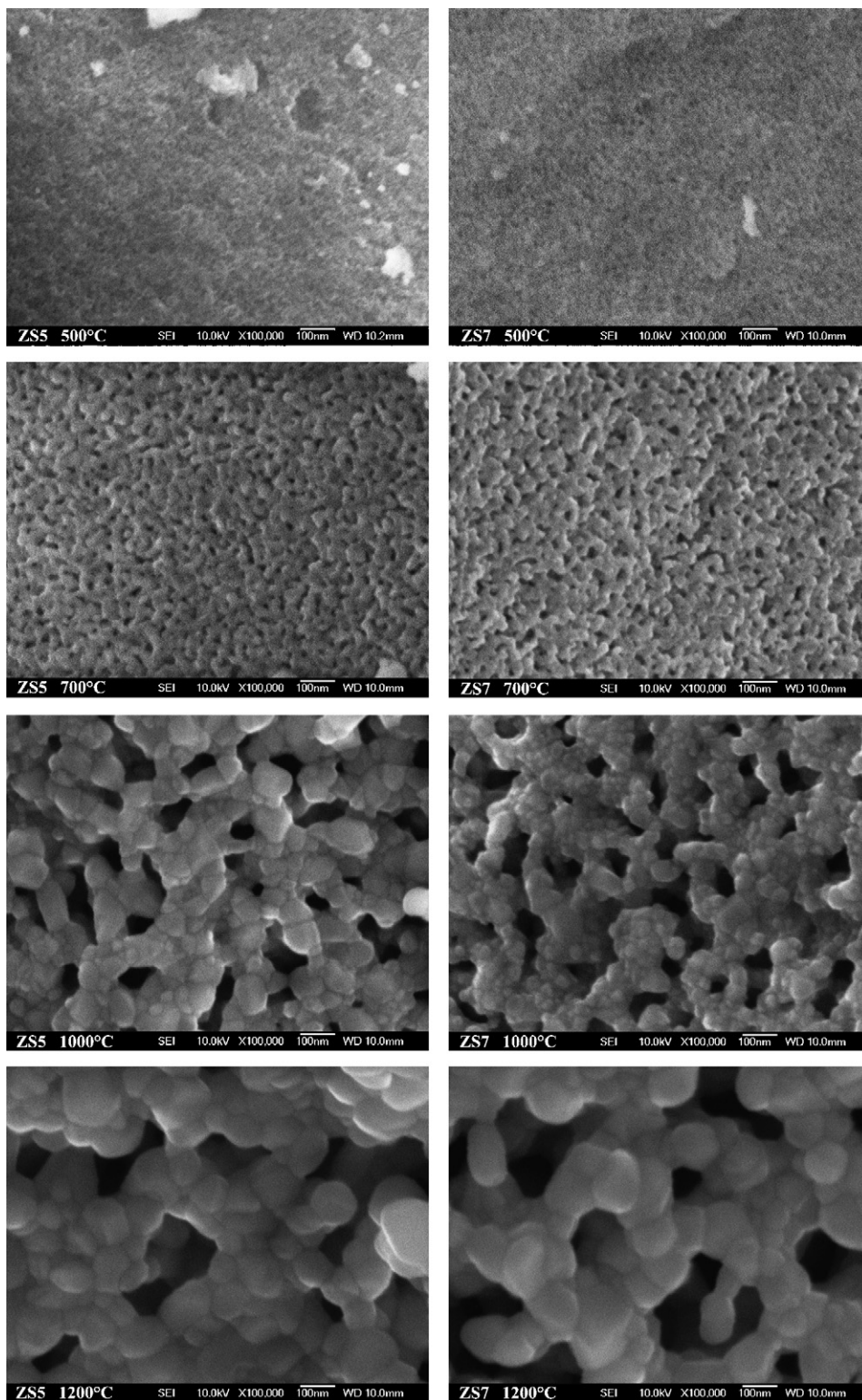


Fig. 13. FE-SEM micrographs of crystallization products from the  $\text{ZrO}_2\text{-SnO}_2$  system with 30 mol% (ZS5) and 50 mol% (ZS7) of  $\text{SnO}_2$  calcined at 500 °C, 700 °C, 1000 °C and 1200 °C.

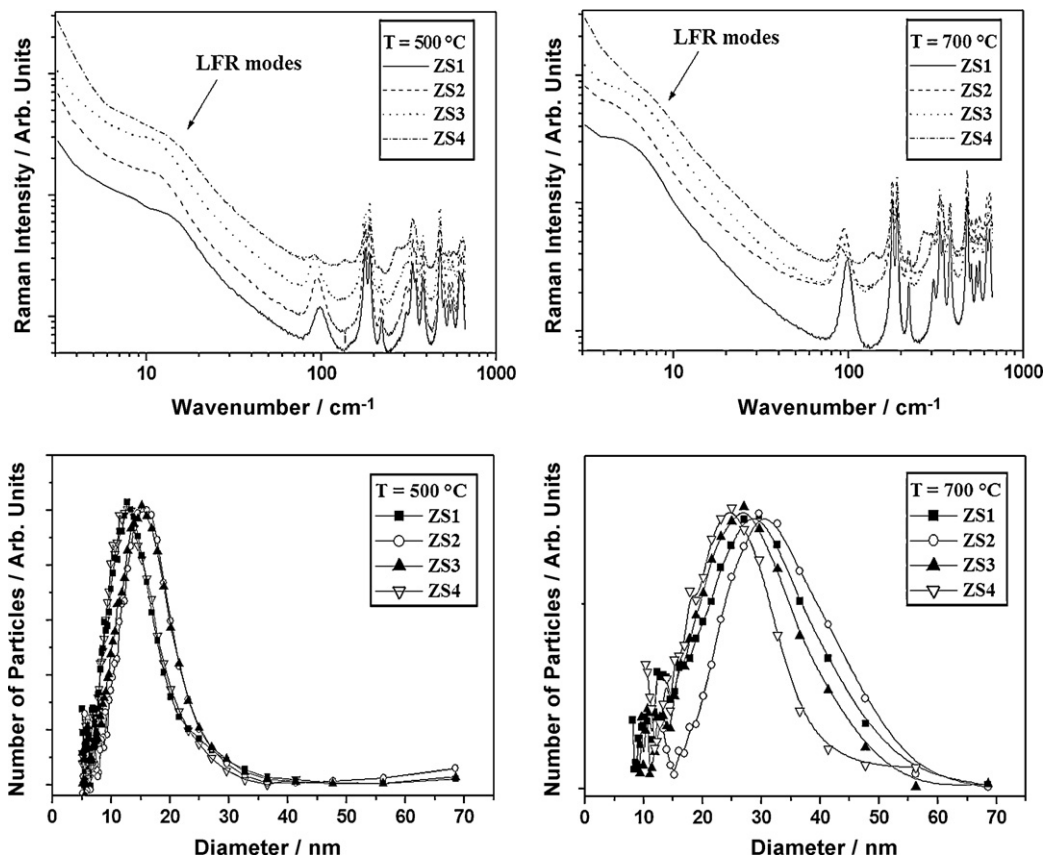


Fig. 14. Low frequency Raman spectra, in log–log coordinates, of the  $\text{ZrO}_2\text{-SnO}_2$  samples calcined at 500 °C (upper left) and 700 °C (upper right). The arrows indicate the position of the particles vibrational modes. Particles size distributions, deduced from the low frequency Raman modes of the samples annealed at 500 °C (down left) and 700 °C (down right) are plotted below.

final result. After subtraction of the background, the size distributions,  $N(D)$ , are calculated from the resulted Raman spectrum by using the relation [33]:

$$N(D) \sim \frac{I(\nu)\nu^2}{n(\nu) + 1} \quad (1)$$

where  $I(\nu)$  is the Raman intensity of the particle vibrational modes (resulted Raman spectrum after subtraction),  $n(\nu)$  is the Bose–Einstein boson occupation factor and  $\nu$  is the frequency. The diameter  $D$  of the particles was calculated by applying a simple substitution of the frequency  $\nu$  of the symmetric vibrational mode with the corresponding diameter  $D = \beta/\nu$ , where the parameter  $\beta$  was deduced from [33]:

$$\beta = \frac{S\nu}{\pi c}. \quad (2)$$

Here  $\nu$  is the longitudinal velocity of sound,  $c$  is the vacuum light velocity, and  $S$  is the constant of the order of unity that depends on the ratio of the longitudinal and transverse velocities of sound within the particle. In order to obtain the values of the sound velocity, the experimental values of the elastic constants of monoclinic  $\text{ZrO}_2$  have been obtained via Brillouin scattering on pure  $\text{ZrO}_2$  [34]. The density of  $6.1 \text{ g cm}^{-3}$  has been assumed for zirconia. The sound velocities of the  $\text{ZrO}_2$  crystal, calculated as a mean value across 7 (for  $\nu_1$ ) and 14 (for  $\nu_t$ ) crystalline sound propagating vectors, are  $\nu_1 = 7380 \text{ m/s}$  and  $\nu_t = 3980 \text{ m/s}$ , respectively. Using the ratio  $\nu_1/\nu_t = 1.89$ , the coefficient  $S = 2.72$  for the symmetric vibrational mode was found. Then, the parameters  $\beta$ , calculated by Eq. (2) for the symmetric mode, is  $2.13 \times 10^{-5}$ . Average particle size of the crystallization products calcined at 500 °C (10–15 nm) and 700 °C (25–

Table 3

Values of the volume-averaged domain size ( $D_v$ ) and upper limits of micro-strain ( $e$ ), estimated from the results of whole-powder-pattern refinements (GSAS program), of the m-ZrO<sub>2</sub>-type solid solutions calcined at 700 °C

	ZS0	ZS1	ZS2	ZS3	ZS4
$D_v$ (nm)	27(1)	24(1)	22(1)	19(1)	16(2)
$e \times 10^3$	1.6(2)	2.4(3)	2.5(3)	3.5(3)	5.8(5)

30 nm), estimated from the corresponding size distribution curves (Fig. 14), appeared to be in good agreement with the results of FE-SEM analysis.

The results of size/strain (line broadening) analysis of XRD patterns of the m-ZrO<sub>2</sub>-type solid solutions calcined at 700 °C are given in Table 3. The increased amount of incorporated Sn<sup>4+</sup> ions caused a gradual decrease in the volume-averaged domain size ( $D_v$ ), from ~27 nm for 0 mol% of SnO<sub>2</sub> to ~16 nm for 20 mol% of SnO<sub>2</sub>, and an increase of upper limits of micro-strains ( $e$ ), from ~0.0016 for 0 mol% of SnO<sub>2</sub> to ~0.0058 for 20 mol% of SnO<sub>2</sub>.

#### 4. Conclusions

The results of DTA analysis show that the crystallization temperature of ZrO<sub>2</sub>-SnO<sub>2</sub> systems increased with an increased SnO<sub>2</sub> content, but the rate of the increase was significantly smaller compared with ZrO<sub>2</sub>-MO<sub>1.5</sub> systems (M stands for trivalent undersized cations). Maximum solubility of Sn<sup>4+</sup> ions in the ZrO<sub>2</sub> lattice was estimated at ~25 mol% (500 °C). The results of phase analysis show that the incorporation of Sn<sup>4+</sup> ions could not stabilize c-ZrO<sub>2</sub> and has little (if any) influence on the stabilization of t-ZrO<sub>2</sub>. The phase structurally closely related to m-ZrO<sub>2</sub> was dominant in all crystallization products having an SnO<sub>2</sub> content below 50 mol%. Crystallization products having an SnO<sub>2</sub> content above the tin solid-solubility limit contain a phase structurally closely related to cassiterite (t-SnO<sub>2</sub>). A rise in the calcination temperature up to 800 °C leads to a decrease in the solid-solubility of Sn<sup>4+</sup> ions followed by an increase in the amount of the phase structurally closely related to t-ZrO<sub>2</sub>. Partial stabilization of metastable t-ZrO<sub>2</sub> in these products probably results from the ZrO<sub>2</sub>-SnO<sub>2</sub> surface interaction that prevents the diffusion of oxygen from the atmosphere into the ZrO<sub>2</sub> lattice and triggers the t-ZrO<sub>2</sub> → m-ZrO<sub>2</sub> transition upon cooling. Further temperature treatments caused a decrease (1000 °C) and disappearance (1200 °C) of the metastable t-ZrO<sub>2</sub>-type phase and an increase of m-ZrO<sub>2</sub>- and t-SnO<sub>2</sub>-type phases. Upon calcination at 1000 °C the crystallization products of samples with 40 or 50 mol% of SnO<sub>2</sub> contained a small amount of the metastable ZrSnO<sub>4</sub> phase, which disappeared on further calcination at 1200 °C.

The results of precise lattice parameters determination, using both Rietveld and Le Bail refinements of powder diffraction patterns, show that the incorporation of Sn<sup>4+</sup> ions caused an asymmetric distortion of the monoclinic ZrO<sub>2</sub> lattice. The increased amount of incorporated Sn<sup>4+</sup> ions causes an increase in parameter  $a$ , a decrease in parameter  $b$ , a very small decrease in parameter  $c$ , and a significant decrease in angle  $\beta$ . However, the unit-cell volume of m-ZrO<sub>2</sub>-type solid solutions remained almost unchanged.

The results of micro-structural analysis show that the sinterability of ZrO<sub>2</sub>-SnO<sub>2</sub> crystallization products significantly decreased with an increase in the SnO<sub>2</sub> content.

#### Acknowledgement

The authors wish to thank Dr. Sc. Rudolf Trojko for his DTA measurements.

#### References

- [1] R. Stevens, Zirconia and Zirconia Ceramics, Magnesium Electron Publication No. 113, Magnesium Electron Ltd., Twickenham, U.K., 1986 (Printed by Litko 2000).
- [2] S.M. Ho, Mater. Sci. Eng. 54 (1982) 23–29.
- [3] K. Tsukuma, M. Shimada, J. Mater. Sci. 20 (1985) 1178–1184.
- [4] V.C. Pandolfelli, J.A. Rodrigues, R. Stevens, J. Mater. Sci. 26 (1991) 5327–5334.
- [5] J. Lefèvre, Ann. Chim. 8 (1963) 117–149.
- [6] P. Li, I.-W. Chen, J.E. Penner-Hahn, J. Am. Ceram. Soc. 77 (1994) 1281–1288.

- [7] B.A. Hunter, C.J. Howard, D.J. Kim, *Aust. J. Phys.* 51 (1998) 539–545.
- [8] B.A. Hunter, C.J. Howard, D.J. Kim, *Physica B* 241–243 (1998) 1249–1251.
- [9] B.A. Hunter, C.J. Howard, D.-J. Kim, *J. Solid State Chem.* 146 (1999) 363–368.
- [10] D.J. Kim, J.W. Jang, H.L. Lee, *J. Am. Ceram. Soc.* 80 (1997) 1453–1461.
- [11] B. Gaillard-Allemand, R. Podor, M. Vilasi, Ch. Rapin, A. Maître, P. Steinmetz, *J. Eur. Ceram. Soc.* 22 (2002) 2297–2303.
- [12] G. Wilson, F.P. Glasser, *Br. Ceram. Trans.* 88 (1989) 69–74.
- [13] S.R. Dhage, V. Samuel, R. Pasricha, V. Ravi, *Ceram. Int.* 32 (2006) 939–941.
- [14] J.C. Ray, R. Saha, P. Pramanik, *Mater. Lett.* 57 (2003) 2140.
- [15] G. Štefanić, B. Gržeta, K. Nomura, R. Trojko, S. Musić, *J. Alloys Compd.* 327 (2001) 151–160.
- [16] G. Štefanić, S. Musić, R. Trojko, *J. Alloys Compd.* 388 (2005) 126–137.
- [17] G. Štefanić, S. Musić, A. Gajović, *J. Mol. Struct.* 744–747 (2005) 541–549.
- [18] G. Štefanić, S. Musić, *J. Alloys Compd.* 460 (2008) 444–452.
- [19] G. Štefanić, S. Popović, S. Musić, *Mater. Lett.* 36 (1998) 240–244.
- [20] A. Le Bail, H. Duroy, J.L. Fourquet, *Mater. Res. Bull.* 23 (1988) 447–452.
- [21] A.C. Larson, R.B. Von Dreele, *General Structure Analysis System GSAS*, Los Alamos National Laboratory Report, 2001.
- [22] B.H. Toby, *J. Appl. Cryst.* 34 (2001) 210–213.
- [23] D. Balzar, N. Audebrand, M. Daymond, A. Fitch, A. Hewat, J.I. Langford, A. Le Bail, D. Louër, O. Masson, C.N. McCowan, N.C. Popa, P.W. Stephens, B. Toby, *J. Appl. Cryst.* 37 (2004) 911–924.
- [24] H.M. Rietveld, *J. Appl. Cryst.* 2 (1969) 65–71.
- [25] L. Lutterotti, S. Matthies, H.-R. Wenk, in: *Proceedings of the 12th International Conference on Textures of Materials (ICOTOM-12)*, vol. 1, 1999, p. 1599.
- [26] H. Toraya, M. Yoshimura, S. Somiya, *J. Am. Ceram. Soc.* 67 (1984) C119–C121.
- [27] H. Toraya, *J. Appl. Cryst.* 19 (1986) 440–447.
- [28] H. Fujimori, M. Yashima, S. Sasaki, M. Kakihana, T. Mori, M. Tanaka, M. Yoshimura, *Chem. Phys. Lett.* 346 (2001) 217–223.
- [29] T. Merle, R. Guinebretiere, A. Mirgorodsky, P. Quintard, *Phys. Rev. B* 65 (2002) (144302-1-144302-6).
- [30] G. Štefanić, S. Musić, A. Gajović, *Mater. Res. Bull.* 41 (2006) 764–777.
- [31] R. Srinivasan, T.R. Watkins, C.R. Hubbard, B.H. Davis, *Chem. Mater.* 7 (1995) 725–730.
- [32] G. Štefanić, M. Didović, S. Musić, *J. Mol. Struct.* 834 (2007) 435–444.
- [33] M. Ivanda, K. Furić, S. Musić, M. Ristić, M. Gotić, D. Ristić, A.M. Tonejc, I. Djerdj, M. Mattarelli, M. Montagna, F. Rossi, M. Ferrari, A. Chiasera, Y. Jestin, G.C. Righini, W. Kiefer, R.R. Gonçalves, *J. Raman Spectrosc.* 38 (2007) 647–659.
- [34] S.-K. Chan, Y. Fang, M. Grimsditch, Z. Li, M.V. Nevitt, W.M. Robertson, E.S. Zouboulis, *J. Am. Ceram. Soc.* 74 (1991) 1742–1744.